Bejan flow visualization of free convection in a Jeffrey fluid from a semi-infinite vertical cylinder : influence of Deborah and Prandtl numbers

Kumar, M, Reddy, GJ and Beg, OA

http://dx.doi.org/10.1007/s10973-019-08099-7

Journal of Thermal Analysis and Calorimetry:

An International Forum for Thermal Studies

ISSN: 1388-6150 (Print) 1588-2926 (Online)

Accepted: 14 February 2019

BEJAN FLOW VISUALIZATION OF FREE CONVECTION IN A JEFFREY FLUID FROM A SEMI-INFINITE VERTICAL CYLINDER: INFLUENCE OF DEBORAH AND PRANDTL NUMBERS

Mahesh Kumar[1], G. Janardhana Reddy[1,*] ***and*** O. Anwar Bég[2]
[1]*Department of Mathematics, Central University of Karnataka, Kalaburagi, India-585367*
[2]*Fluid Mechanics, Aeronautical and Mechanical Engineering Department, School of Computing, Science and Engineering, University of Salford, Manchester M54WT, UK.*
**** Corresponding author - Email:*** **gjr@cuk.ac.in**

Abstract:

This article studies the pattern of heat lines in free convection non-Newtonian flow from a semi-infinite vertical cylinder via Bejan's heat function concept. The viscoelastic Jeffrey fluid model is employed. The time-dependent, coupled, non-linear conservation equations for momentum and energy (heat) are solved computationally with the unconditionally stable finite difference Crank-Nicolson method. Extensive graphical results are presented for the influence of Deborah number (viscoelastic parameter) and Prandtl number (with ranges 0 - 0.8 and 0.68 - 7.2, respectively) on thermal and flow characteristics including time histories of overall skin-friction and heat transfer rate. Lower values of Deborah number indicate that the material acts in a more fluid-like manner whereas the higher values of Deborah number correspond to the material showing characteristics more associated with a solid. The solutions indicate that the time taken for the flow-field variables to achieve the steady-state is increased with higher values of Deborah number. Boundary flow visualization is presented using heat lines, isotherms and streamlines. It is observed that as Deborah number increases the intensity of heat lines increases and they tend to deviate from the hot cylindrical wall. Furthermore, the flow-field variables for the Newtonian fluid case exhibit a significantly different pattern from that of Jeffrey fluid.

Keywords*:* *Jeffrey fluid; Heat lines; Vertical cylinder; Implicit method; Deborah number.*

1.INTRODUCTION

The study of exterior boundary layer flows with heat transfer is fundamental to numerous processes arising in materials fabrication, chemical processing and manufacturing systems. In most engineering systems the surface is curved. Typical configurations include conical bodies, spheres, ellipses, toroids, curved ducts and cylinders. In particular, the cylinder features in numerous convective flow operations includes tubular flows, heat exchangers, membrane-based separation modules, filtration screens used for clarifying suspensions, coating of wires, mixing processes, polymer fiber spinning, food stuff synthesis, nanotechnology etc. Such geometries have stimulated considerable interest in engineering analysis and a number of investigations have presented solutions for momentum and heat transfer features from cylinders with different cross-sections. [1-5].

Research on the flow of a non-Newtonian fluid with heat transfer is also a fervent area of endeavour owing to abundant industrial applications. These fluids show shear-stress-strain relationships which differ considerably from the standard Newtonian model. Many studies have been communicated for transport phenomena in non-Newtonian fluids [6-10]. These studies feature diverse mathematical models to characterize the behaviour of non-Newtonian fluids. Examples of non-Newtonian fluids include coal in water, synthetic lubricants, pulps, molten plastics, polymers, ink, glues, emulsions, etc. Some technologies in which such fluids are deployed include energy systems, chemicals, cosmetics, polymer processing, pharmaceuticals, biotechnology, surface coating of machine components, automotive body forming etc. Free convection flows of non-Newtonian fluids have also generated substantial attention and an extensive spectrum of rheological models have been utilized including viscoelastic, visco-plastic, microstructural and memory fluids. Turan *et al.* [11] analysed two-dimensional laminar free convection in an enclosure occupied with non-Newtonian fluids with differentially heated sidewalls. Kim *et al.* [12] have analysed the time-dependent natural convection in a square enclosure containing power-law fluids. Recently, Sheremet and Pop [13] analysed the flow of viscoelastic fluid in a square cavity. Further, Reddy *et al.* [14] studied the non-Newtonian thermal convection from a vertical cylinder numerically with entropy generation. Using finite difference scheme, Reddy *et al.* [15] analysed the flow of a non-Newtonian fluid with MHD effects from a vertical plate.

In the view of the very complex range of behaviours observed in viscoelastic non-Newtonian fluids, many different constitutive formulations have been developed in the literature. A popular subclass of elastic-viscous models is the Jeffrey fluid [16-21] which includes important characteristics of retardation and relaxation times. In fact, this model is a

comparatively simple linear model that uses the time derivative rather than convective derivative. When subjected to stress a Jeffrey fluid is deformed; however, when stress is eliminated, the deformation does not vanish immediately like Newtonian fluids. In this fluid, the interior molecular configuration can endure stress for a certain time. Therefore, this Jeffrey fluid model has received considerable attention in mathematical modelling. Recently, Hayat *et al*. [22] studied the Jeffrey fluid boundary layer flow over an impermeable inclined stretching cylinder with heat transfer. Incompressible Jeffrey flow and heat transfer between coaxial cylinders was investigated by Malik *et al.* [23]. Prasad *et al.* [24] studied numerically the thermal convection boundary layer flow from a cylinder to a Jeffery fluid with the Keller box scheme. Sreenadh *et al.* [25] investigated the free convective Jeffery fluid flow in a vertical porous stratum.

In thermal flow simulation, a very powerful tool is fluid-flow and temperature contour visualization which is achieved usually with the assistance of isotherms and streamlines. The isotherms are used to exemplify the temperature field distribution in a given region. However, they are unable to quantify in sufficient details the actual energy flow pathways. Particularly in convective heat transport problems, due to pure conduction, the heat flux direction is non-orthogonal to that of the temperature contours. In such situations, the heat lines are the best way to visualize heat transfer in two-dimensional convective transport processes. These will provide the path for transfer of energy which occurs from hot to cold walls. Initially, the concept of *heat line visualization* was developed by Kimura and Bejan [26] and Bejan [27]. For open cavities, Bondareva *et al.* [28-29] examined the heat lines visualization for natural convective with nanofluid. Pratibha *et al.* [30] studied the visualization of heat lines in mixed convection flows within a triangular cavity. Using the same idea, Monisha *et al.* [31] conducted heat line visualization in a cavity with a moving horizontal wall. Recently, Vinay *et al.* [32] numerically studied the heat line and mass line visualization in an enclosure. Also, Reddy *et al.* [33] examined the heat line visualization for non-Newtonian fluid from a hollow cylinder. The deployment of the heat lines methodology for convection problems is further elucidated in [34]. Thus far however the heat lines visualization has not been studied widely in non-Newtonian heat transfer simulations and has been neglected for the case of the Jeffrey viscoelastic fluid. Furthermore, an inspection of literature reveals that relatively limited analysis has been presented so far, for time-dependent flows of elastic-viscous Jeffrey fluid from a vertical cylinder. Hence the current work presents, *for the first time, accurate and detailed*

visualization of unsteady boundary layer thermal convection flow of a Jeffrey fluid from a uniform vertical cylinder by means of the Bejan heat function concept. The mathematical model developed in the next section is non-dimensionalized and then solved with a Crank-Nicolson finite difference method. Validation with earlier studies (Newtonian) is included. Extensive graphical results are presented for the influence of the viscoelastic parameter (Deborah number), Prandtl number and also Jeffery rheological parameter on heat and momentum characteristics. The current study has to the authors' knowledge not appeared anywhere in the literature and constitutes a novel contribution to modelling aspects of for example thermal polymer processing.

2. MATHEMATICAL FORMULATION

Consider time-dependent two-dimensional incompressible buoyancy-driven flow of a Jeffrey viscoelastic fluid from a heated vertical cylinder. The cylinder has radius r_0 and is depicted in **Fig. 1**. A rectangular coordinate system is adopted in which the *x*-axis and *r*-axis are considered to be vertically upward and normal to the cylinder. The neighbouring fluid temperature is static and analogous to the ambient temperature T'_∞. At the initiation of flow, i.e., $t' = 0$, the temperature T'_∞ is identical for the cylinder and the neighbouring fluid. Soon after ($t' > 0$), the cylinder temperature is amplified to T'_w ($> T'_\infty$) and maintained consistently there afterward. The constitutive equations for viscous incompressible Jeffrey viscoelastic fluid are:

$$\overline{T} = P\overline{I} + \overline{S} \text{ and } \overline{S} = \frac{\mu}{1+\lambda}\left(\dot{\overline{\gamma}} + \lambda_1 \ddot{\overline{\gamma}}\right) \tag{1}$$

Here all terms are defined in the nomenclature. Incorporating the appropriate shear stress terms from Eqn (1), the problem under study may be described by the following governing equations for mass, momentum and energy conservation under the Boussinesq approximation [20, 35, 36]:

$$\frac{\partial(ru)}{\partial x} + \frac{\partial(rv)}{\partial r} = 0 \tag{2}$$

$$\frac{\partial u}{\partial t'} + u\frac{\partial u}{\partial x} + v\frac{\partial u}{\partial r} = \frac{\nu}{1+\lambda}\left[\frac{\partial^2 u}{\partial r^2} + \frac{1}{r}\frac{\partial u}{\partial r} + \lambda_1\left(\begin{array}{l}\frac{\partial^3 u}{\partial r^2 \partial t'} + \frac{\partial v}{\partial r}\frac{\partial^2 u}{\partial r^2} + v\frac{\partial^3 u}{\partial r^3} + \frac{\partial u}{\partial r}\frac{\partial^2 u}{\partial x \partial r} \\ + u\frac{\partial^3 u}{\partial x \partial r^2} + \frac{1}{r}\frac{\partial^2 u}{\partial r \partial t'} + \frac{v}{r}\frac{\partial^2 u}{\partial r^2} + \frac{u}{r}\frac{\partial^2 u}{\partial x \partial r}\end{array}\right)\right] + \mathrm{g}\beta_T(T' - T'_\infty) \tag{3}$$

$$\frac{\partial T'}{\partial t'} + u\frac{\partial T'}{\partial x} + v\frac{\partial T'}{\partial r} = \frac{\alpha}{r}\frac{\partial}{\partial r}\left(r\frac{\partial T'}{\partial r}\right) \tag{4}$$

The above system is closed by the following conditions:

$$\begin{aligned} &t' \le 0: T' = T'_\infty, u = 0, v = 0, && \text{for all } x \text{ and } r \\ &t' > 0: T' = T'_w, u = 0, v = 0, && \text{at } r = r_0 \\ &\quad T' = T'_\infty, u = 0, v = 0 && \text{at } x = 0 \\ &\quad T' \to T'_\infty, u \to 0, \frac{\partial u}{\partial r} \to 0, v \to 0 && \text{at } r \to \infty \end{aligned} \tag{5}$$

Invoking the following non-dimensional quantities (for all symbols refer to the nomenclature) [37, 38]:

$X = Gr^{-1}\frac{x}{r_0}$, $R = \frac{r}{r_0}$, $U = Gr^{-1}\frac{ur_0}{\upsilon}$, $V = \frac{vr_0}{\upsilon}$, $t = \frac{\upsilon t'}{r_0^2}$, $\theta = \frac{T'-T'_\infty}{T'_w-T'_\infty}$, $Gr = \frac{g\beta_T r_0^3(T'_w-T'_\infty)}{\upsilon^2}$, $Pr = \frac{\upsilon}{\alpha}$, $\beta = \lambda_1\upsilon/r_0^2$,

Insertion of the above relations into the governing Eqns. (2) - (5), leads to the following system of partial differential boundary layer equations:

$$\frac{\partial U}{\partial X} + \frac{\partial V}{\partial R} + \frac{V}{R} = 0 \tag{6}$$

$$\frac{\partial U}{\partial t} + U\frac{\partial U}{\partial X} + V\frac{\partial U}{\partial R} = \theta + \frac{1}{1+\lambda}\left[\frac{\partial^2 U}{\partial R^2} + \frac{1}{R}\frac{\partial U}{\partial R} + \beta\left(\begin{array}{c}\frac{\partial^3 U}{\partial R^2\partial t} + \frac{\partial V}{\partial R}\frac{\partial^2 U}{\partial R^2} + V\frac{\partial^3 U}{\partial R^3} + \frac{\partial U}{\partial R}\frac{\partial^2 U}{\partial X\partial R} \\ +U\frac{\partial^3 U}{\partial X\partial R^2} + \frac{1}{R}\frac{\partial^2 U}{\partial R\partial t} + \frac{V}{R}\frac{\partial^2 U}{\partial R^2} + \frac{U}{R}\frac{\partial^2 U}{\partial X\partial R}\end{array}\right)\right] \tag{7}$$

$$\frac{\partial \theta}{\partial t} + U\frac{\partial \theta}{\partial X} + V\frac{\partial \theta}{\partial R} = \frac{1}{Pr}\left(\frac{\partial^2 \theta}{\partial R^2} + \frac{1}{R}\frac{\partial \theta}{\partial R}\right) \tag{8}$$

The corresponding initial and boundary conditions are:

$$\begin{aligned} &t \le 0: \theta = 0, U = 0, V = 0 && \text{for all } X \text{ and } R \\ &t > 0: \theta = 1, U = 0, V = 0 && \text{at } R = 1; \\ &\quad \theta = 0, U = 0, V = 0 && \text{at } X = 0 \\ &\quad \theta \to 0, U \to 0, \frac{\partial U}{\partial R} \to 0, V \to 0 && \text{as } R \to \infty \end{aligned} \tag{9}$$

3. NUMERICAL SOLUTION

The unsteady coupled non-linear Eqs. (6) - (8) are evaluated by Crank-Nicolson finite difference scheme and the corresponding finite difference equations are:

$$\frac{U_{i,j}^{k+1}-U_{i-1,j}^{k+1}+U_{i,j}^{k}-U_{i-1,j}^{k}}{2\Delta X}+\frac{V_{i,j}^{k+1}-V_{i,j-1}^{k+1}+V_{i,j}^{k}-V_{i,j-1}^{k}}{2\Delta R}+(JR)V_{i,j}^{k+1}\ =\ 0 \tag{10}$$

$$\frac{U_{i,j}^{k+1}-U_{i,j}^{k}}{\Delta t}+\frac{U_{i,j}^{k}}{2\Delta X}\left(U_{i,j}^{k+1}-U_{i-1,j}^{k+1}+U_{i,j}^{k}-U_{i-1,j}^{k}\right)+\frac{V_{i,j}^{k}}{4\Delta R}\left(U_{i,j+1}^{k+1}-U_{i,j-1}^{k+1}+U_{i,j+1}^{k}-U_{i,j-1}^{k}\right)$$
$$=\frac{\theta_{i,j}^{k+1}+\theta_{i,j}^{k}}{2}+\frac{JR}{1+\lambda}\left[\frac{U_{i,j+1}^{k+1}-U_{i,j-1}^{k+1}+U_{i,j+1}^{k}-U_{i,j-1}^{k}}{4(\Delta R)}\right]+\frac{1}{1+\lambda}\left[\frac{U_{i,j+1}^{k+1}-2U_{i,j}^{k+1}+U_{i,j-1}^{k+1}+U_{i,j+1}^{k}-2U_{i,j}^{k}+U_{i,j-1}^{k}}{2(\Delta R)^{2}}\right]$$
$$+\frac{\beta}{1+\lambda}\left[\frac{\left(V_{i,j+1}^{k+1}-V_{i,j-1}^{k+1}+V_{i,j+1}^{k}-V_{i,j-1}^{k}\right)\left(U_{i,j+1}^{k+1}-2U_{i,j}^{k+1}+U_{i,j-1}^{k+1}+U_{i,j+1}^{k}-2U_{i,j}^{k}+U_{i,j-1}^{k}\right)}{8(\Delta R)^{3}}\right]$$
$$+\frac{\beta V_{i,j}^{k}}{1+\lambda}\left[\frac{\left(U_{i,j+2}^{k+1}-2U_{i,j+1}^{k+1}+2U_{i,j-1}^{k+1}+U_{i,j-2}^{k+1}+U_{i,j+2}^{k}-2U_{i,j+1}^{k}+2U_{i,j-1}^{k}+U_{i,j-2}^{k}\right)}{4(\Delta R)^{3}}\right]$$
$$+\frac{\beta}{1+\lambda}\left[\frac{U_{i,j+2}^{k+1}-2U_{i,j}^{k+1}+U_{i,j-2}^{k+1}-U_{i,j+2}^{k}+2U_{i,j}^{k}-U_{i,j-2}^{k}}{4(\Delta R)^{2}\Delta t}\right]+\frac{(JR)\beta}{1+\lambda}\left[\frac{U_{i,j+1}^{k+1}-U_{i,j-1}^{k+1}+U_{i,j-1}^{k}-U_{i,j+1}^{k}}{2(\Delta R)\Delta t}\right]$$
$$+\frac{\beta}{1+\lambda}\left[\frac{\left(U_{i,j+1}^{k}-U_{i,j-1}^{k}\right)\left(U_{i,j+1}^{k+1}-U_{i-1,j+1}^{k+1}-U_{i,j-1}^{k+1}+U_{i-1,j-1}^{k+1}+U_{i,j+1}^{k}-U_{i-1,j+1}^{k}-U_{i,j-1}^{k}+U_{i-1,j-1}^{k}\right)}{8(\Delta R)^{2}\Delta X}\right]$$
$$+\frac{\beta U_{i,j}^{k}}{1+\lambda}\left[\frac{\left(U_{i,j+1}^{k+1}-U_{i-1,j+1}^{k+1}-2U_{i,j}^{k+1}+2U_{i-1,j}^{k+1}+U_{i,j-1}^{k+1}-U_{i-1,j-1}^{k+1}+U_{i,j+1}^{k}-U_{i-1,j+1}^{k}-2U_{i,j}^{k}+2U_{i-1,j}^{k}+U_{i,j-1}^{k}-U_{i-1,j-1}^{k}\right)}{2(\Delta R)^{2}\Delta X}\right]$$
$$+\frac{(JR)\beta V_{i,j}^{k}}{1+\lambda}\left[\frac{U_{i,j+1}^{k+1}-2U_{i,j}^{k+1}+U_{i,j-1}^{k+1}+U_{i,j+1}^{k}-2U_{i,j}^{k}+U_{i,j-1}^{k}}{2(\Delta R)^{2}}\right]$$
$$+\frac{(JR)\beta U_{i,j}^{k}}{1+\lambda}\left[\frac{U_{i,j+1}^{k+1}-U_{i-1,j+1}^{k+1}-U_{i,j-1}^{k+1}+U_{i-1,j-1}^{k+1}+U_{i,j+1}^{k}-U_{i-1,j+1}^{k}-U_{i,j-1}^{k}+U_{i-1,j-1}^{k}}{4(\Delta R)\Delta X}\right] \tag{11}$$

$$\frac{\theta_{i,j}^{k+1}-\theta_{i,j}^{k}}{\Delta t}+\frac{U_{i,j}^{k}}{2\Delta X}\left(\theta_{i,j}^{k+1}-\theta_{i-1,j}^{k+1}+\theta_{i,j}^{k}-\theta_{i-1,j}^{k}\right)+\frac{V_{i,j}^{k}}{4\Delta R}\left(\theta_{i,j+1}^{k+1}-\theta_{i,j-1}^{k+1}+\theta_{i,j+1}^{k}-\theta_{i,j-1}^{k}\right)=$$
$$\left[\frac{\theta_{i,j+1}^{k+1}-2\theta_{i,j}^{k+1}+\theta_{i,j-1}^{k+1}+\theta_{i,j+1}^{k}-2\theta_{i,j}^{k}+\theta_{i,j-1}^{k}}{2Pr(\Delta R)^{2}}\right]+(JR)\left[\frac{U_{i,j+1}^{k+1}-U_{i,j-1}^{k+1}+U_{i,j+1}^{k}-U_{i,j-1}^{k}}{4\mathrm{Pr}(\Delta R)}\right] \tag{12}$$

where, $JR=\frac{1}{[1+(J-1)\Delta R]}$. The methodology to solve the above equations is explained at length in [15, 38]. The region of integration with $X_{min}=0, X_{max}=1, R_{min}=1$ and $R_{max}(=\infty)=20$ is considered with R_{max} far from the boundary layer edges. It is seen that 100×500 grid compared with 50×250 and 200×1000 does not have a significant effect on the results of steady-state flow variables which are shown in the **Fig. 2**. Hence according to this observation, a

uniform grid size of 100 X 500 is of sufficient accuracy for this study with the mesh sizes of 0.01 and 0.03, respectively. Also, to produce reliable results, the time-step sensitivity analysis has been conducted for various time-step sizes and is summarized in **Table 3**. The effective time-step size Δt $(t = k\Delta t, k = 0, 1, 2, \ldots)$ is fixed as 0.01 for numerical computations.

4. RESULTS AND DISCUSSION

The correctness of the numerical results is checked by relating the present results with reported by Lee *et al.* [5], for air (Pr = 0.71), $\beta = 0$ and $\lambda = 0$ and shown in **Fig. 3**. Both results match well. The simulated non-dimensional flow variables, average heat transfer coefficients and wall shear stress are analysed in detail in the following subsections along with streamlines, heat lines and isotherms for different physical parameters values such as Deborah number (β) and Prandtl number (Pr). Such type of variations is shown graphically and discussed in the following subsections. Also, in this problem the Deborah number, β $(= \frac{\lambda_1 v}{{r_0}^2})$ is the ratio of the characteristic time to the time-scale of deformation. If $\beta > 0.1$ the elastic effects are dominant and the material follows viscoelastic behaviour whereas if $\beta < 0.1$ then viscous effects prevail. Hence for analysing the Jeffrey fluid flow model, we consider $\beta > 0.1$ values with fixed Jeffrey fluid parameter (λ=1.0) in the present research paper. Similarly, the Prandtl number values 0.68 and 7.2 signify the hydrogen and sea water, respectively. Thermal diffusivity dominates for lower value of Pr and for higher Pr the momentum diffusivity dominates the behaviour.

3.1 Flow variables

The velocity (U) graph at two distinct locations, i.e., (1, 1.19) and (1, 3.09) for various Pr and β with fixed λ values are drawn against t, and which are shown graphically in **Figure 4**. The velocity graphs depicted in Figs. 4(a-b) are drawn in the vicinity of and distant from the hot cylinder wall, respectively. It can be seen that the velocity at all the position upsurges with t, accomplishes the temporal maxima, and at the end reaches the asymptotic time-independent state. From Fig. 4a and 4b, it is clearly identified that for Pr value 0.68, the velocity declines as β increases. Also, augmenting value of β or Pr, results in the velocity magnitudes for the Jeffrey fluid being markedly lower than for the Newtonian fluid. Further for the case of the Newtonian fluid $(\beta = 0, \lambda = 0)$ and Pr = 0.68, the wall velocity is enhanced with time

monotonically, fluctuates, accomplishes the temporal peak, and becomes asymptotically steady. The time taken for attaining the temporal peak of the velocity and the time-independent state upsurges with enhancing Pr or β. Further, when β is increased, the time required to achieve the temporal peak is *elevated* whereas the time to reach the time-independent state *decreases.* When $\beta > 0.3$ and Pr = 0.68 the velocity magnitudes for the Newtonian fluid exceed those of the Jeffrey fluid whereas when Pr = 7.2 this trend is opposite. Evidently the Prandtl number (ratio of momentum and thermal diffusivity) exerts a significant impact on velocity field and can therefore contribute to flow deceleration or acceleration of the viscoelastic fluid. For the second location (Fig.4b) for the values of β and Pr the time-dependent velocity values of the Newtonian fluid are consistently in excess of the Jeffrey fluid i.e. the viscoelastic fluid exhibits flow deceleration.

The time-independent state velocity versus normal coordinate R for all values of the physical parameters is plotted in **Fig.5.** Here, the U curves commence with zero velocity then ascend to peak values, thereafter, plummeting to zero again, in consistency with the far field boundary conditions (vanishing free stream velocity). The deviation of the Jeffrey fluid U profiles from the hot wall is noticed to be less compared to that of the Newtonian U profiles. It is also manifest that, in close proximity to the hot wall the magnitude of the velocity of the Jeffrey fluid appears larger than for the Newtonian fluid whereas far from the heated wall (cylinder surface) this behaviour is opposite. Hence from this graph, it is identified that for different β steady-state velocity profile for Jeffrey fluid are completely different as compared to Newtonian profiles. This result is due to the fact that at lower values of Deborah number, the material acts in a more fluid-like manner i.e. greater viscous behaviour akin to Newtonian liquids. At higher values of Deborah number, however, the material behaviour enters into the non-Newtonian fluid regime, dominated increasingly by elasticity showing characteristics more associated with a solid. Also, it is noted that from the hot wall the deviation of the velocity profiles is less for the Jeffrey fluid compared to the general Newtonian fluid.

The transient temperature profiles(θ) at a particular location (1, 1.15) for various values of Deborah number (β) and Prandtl number (Pr) with constant λ are depicted in **Fig. 6**. It is pertinent to note that in the Jeffrey fluid model, λ is the ratio of relaxation and retardation times and λ_1 is the retardation time. In the present study however, these parameters are fixed as they have been addressed for both internal and external flows in numerous other studies including Tripathi and Bég [39], Prasad *et al.* [40], Prasad *et al*. [41] and Tripathi *et al*. [42]. To conserve space, the temperature profiles at other locations are not shown since they also exhibit similar

transient behaviour. The temperature profiles in these graphs initially increase with time steadily and after reaching the temporal peak they become asymptotically steady. Temperature profiles decrease as *Pr* increases or β decreases since fluids with higher Prandtl number have lower thermal conductivities implying a suppression in thermal diffusion into the fluid and greater heat transfer to the boundary (cylindrical surface). Also, it interesting to note that these profiles with respect to Jeffrey fluid primarily overlap with the Newtonian fluid and then exhibit divergence from the Newtonian case with progressively greater elapse in time. In particular when *Pr* = 7.2, the Jeffrey fluid θ profile deviates substantially from the profile for the Newtonian fluid at *t* = 7.68. Thus, during the initial time level, the Jeffrey fluid exhibits similar characteristics to Newtonian fluids. The time required to achieve the temporal peak of the temperature requires high values of Deborah number (β) while for a fixed value of *Pr*, this maximum value decreases as β increases. As *Pr* upsurges, the transient temperature value is reduced and it is evidently greater for the Jeffrey fluid compared with the Newtonian fluid.

Temperature profiles at steady-state for constant ratio of relaxation and retardation times (λ) and different values *Pr* and β are shown in **Figure 7**. At all-time values, these profiles begin with the hot wall temperature i.e., θ = 1 and decrease monotonically to zero temperature along the *R* coordinate. Also, the time required to attain the steady-state is enhanced for increasing β and also give rise to thicker profiles. The opposite trend is apparent for a higher value of *Pr*. When *Pr* is high, instead of thermal diffusion, the momentum diffusion dominates, and this affects the behaviour near and at distance from the hot wall. Furthermore, it is identified that the θ profiles for the Jeffrey fluid ($\beta, \lambda > 0$) vary considerably as compared to the Newtonian fluid ($\beta = 0, \lambda = 0$).

3.2 Average wall and heat transfer coefficients

The *non-dimensional wall shear stress and heat transfer rate* are given, respectively by:

$$\overline{C_f} = \int_0^1 \left(\frac{\partial U}{\partial R}\right)_{R=1} dX \tag{13}$$

$$\overline{Nu} = -\int_0^1 \left(\frac{\partial \theta}{\partial R}\right)_{R=1} dX \tag{14}$$

The effects of *Pr* and β (for constant λ) on $\overline{C_f}$ are shown graphically in **Fig. 8**. For all values of *Pr* and β, $\overline{C_f}$ increases with time and eventually the fluctuations are damped out and the skin friction exhibits steady-state asymptotically smooth behaviour. Also, for increasing value

of β, the $\overline{C_f}$ magnitudes are enhanced (flow acceleration) and the reverse tendency (flow retardation) is observed with increasing the *Pr*. In particular it is seen that as *Pr* is elevated the value of $\overline{C_f}$ is increased for the Jeffery fluid compared to that of Newtonian fluid.

Figure 9 depicts the influence of *Pr* and β on $\overline{Nu}$. Increasing the β value leads to a decrement in $\overline{Nu}$ and as *Pr* value increases, the $\overline{Nu}$ (heat transfer rate at the cylinder wall) for the Jeffrey fluid is lower as compared with $\overline{Nu}$ for the Newtonian fluid. Also, for fixed β (= 0.3) the $\overline{Nu}$ magnitudes are markedly augmented with the rising values of *Pr*.

4.3 STREAM AND HEAT FUNCTIONS

The fluid flow visualization patterns are simulated with the stream function ψ, which satisfies continuity equation i.e., Eqn. (6). The stream function ψ related to velocity components *U*, *V* for two-dimensional flows is given as:

$$U = \frac{1}{R}\frac{\partial \psi}{\partial R} \qquad \text{and} \qquad V = -\frac{1}{R}\frac{\partial \psi}{\partial X} \tag{15}$$

Eqn. (15) leads to the following equation and boundary conditions:

$$\frac{\partial^2 \psi}{\partial X^2} + \frac{\partial^2 \psi}{\partial R^2} = U + R\frac{\partial U}{\partial R} - R\frac{\partial V}{\partial X} \tag{16}$$

The no-slip condition is valid at all boundaries as there is no cross flow, hence $\psi = 0$ is used as a boundary condition. i.e. $\psi = \frac{\partial \psi}{\partial X} = 0$ at $X = 0$ and $X = 1(X_{max})$, $\psi = \frac{\partial \psi}{\partial R} = 0$ at $R = 1$, $\frac{\partial \psi}{\partial R} \to 0$ as $R \to \infty$. Also, the heat function (Θ') is defined in terms of first-order derivatives as:

$$\frac{\partial \Theta'}{\partial x} = \rho r v c_p (T' - T'_\infty) - k_1 r \frac{\partial T'}{\partial r} \tag{17a}$$

$$-\frac{1}{r}\frac{\partial \Theta'}{\partial r} = \rho u c_p (T' - T'_\infty) \tag{17b}$$

Here Θ'satisfies the thermal Eqn. (4). The dimensionless heat function $\Omega = \frac{\Theta'}{k_1(T'_w - T'_\infty) r_0 Gr}$ and non-dimensionality is achieved so that its higher value equals the $\overline{Nu}$ on the hot wall [26] and equations (17a) and (17b) can then be rewritten as:

$$\frac{\partial \Omega}{\partial X} = Pr(RV\theta) - R\frac{\partial \theta}{\partial R} \tag{18a}$$

$$-\frac{\partial \Omega}{\partial R} = Pr(RU\theta) \qquad (18b)$$

It is easy to verify that equations (18a) and (18b) identically satisfy the *steady-state* form of energy Eq. (8) and using these equations, one can derive the *Poisson equation* which gives the *heat function field*.

$$\frac{\partial^2 \Omega}{\partial X^2} + \frac{\partial^2 \Omega}{\partial R^2} = Pr\left[R\frac{\partial (V\theta)}{\partial X} - R\frac{\partial (U\theta)}{\partial R} - U\theta\right] - R\frac{\partial^2 \theta}{\partial X \partial R} \qquad (19)$$

The boundary conditions for the heat function (Ω) are taken directly from Eqns. (18a) and (18b), i.e.,

$\Omega(0,0) = 0$,

$\frac{\partial \Omega}{\partial X} = \frac{\partial \Omega}{\partial R} = 0$ at $X = 0$,

$\Omega = -\int_{X=0}^{1}\left(\frac{\partial \theta}{\partial R}\right) dX = \overline{Nu}$ at $R = 1$ and

$\frac{\partial \Omega}{\partial R} \to 0$ as $R \to \infty$.

The values of ψ *and* Ω, are evaluated with the help of second-order finite difference formulae. The steady-state temperature contours, streamlines, and heat lines are depicted in **Fig. 10** for different values of Deborah number (β) with fixed *Pr* and λ. It is evident that the variation of heat lines occurs closer to the hot wall than for the isotherms and streamlines. Noting that velocity satisfies the *no-slip* condition at the cylinder wall, Fig. 10(a), implies that the streamlines are compressed around the foremost edge of the cylinder and the maximum velocity occurs here. Hence, the heat lines in the vicinity of the cylinder wall are perceived to be thicker for small *X* values. Also, the relevant fluid flow and heat transport phenomena occur inside the thermal boundary layer, in consistency with boundary layer theory [43]. The heat lines depict the heat extraction *from the hot wall.* The *heat lines* denote the well-bordered corridors where the heat is transported. The *heat function* contours designate the surrounding pathways, and these are effective tools for visualizing rate of heat transfer rather than the isotherm lines. It is further noted that the isotherms presented in Fig. 10(b), are analysed by the temperature echelons in the thermal region; on the other hand, they are weak and inadequate tools for understanding the concept of *heat flow visualization* and analysis. Hence the study of heat lines is significant for achieving an improved understanding of heat transfer visualization and can be observed in Fig. 10(c). As β is increased, the maximum value of the heat function Ω is

reduced, since the $\overline{Nu}$ decreases on the hot wall (R=1) as shown in **Table 2**. The heat lines observed to be closer to the hot wall for higher values of β, whereas the converse trend is noted for the isotherms.

4.4 Difference between the flow of Jeffrey and Newtonian fluids

Figure 11 visualizes the velocity and temperature variable contours for the non-Newtonian Jeffrey and Newtonian fluid. The Jeffrey fluid velocity curve achieves lower magnitudes than the Newtonian fluid, which may be attributable to the occurrence in the Jeffrey fluid model of additive diffusion terms as given in Eqn. (8). Also, it is seen that the *time-independent* state temperature contours for the Jeffrey fluid attain a thicker temperature layer as compared to those of the Newtonian fluid.

Table 1 explains the difference between Jeffrey fluid (Table 1(a)) and Newtonian fluid (Table 1(b)) flows with respect to velocity and temperature in terms of the temporal peak and the steady-state values, at two distinct locations. It is identified that times taken for the flow-field variables to attain the temporal peak and steady-state are increased with amplifying values of *Pr* and β. Also, for all values of *Pr* and β, the time required to attain the temporal peak and steady-state of all flow variables for the Jeffrey fluid is higher than the Newtonian fluid. Further, for a small value of *Pr*, the maximum velocities occur at X = 1.0. These values for Jeffrey fluid are smaller compared to Newtonian fluid. However, for higher *Pr* values this trend is reversed.

Table 2 compares $\overline{C_f}$ and $\overline{Nu}$ values for the Jeffrey fluid (Table 2(a)) and Newtonian fluid (Table 2(b)) with fixed λ value. It is noticed that for each value of *Pr* and β the average friction factor $\overline{C_f}$ of a Jeffrey fluid attains larger values whereas for Newtonian fluid it shows lower values. The contrary behaviour is computed for the average heat transfer coefficient $\overline{Nu}$. In short, the viscoelastic characteristic induces significant deviation in both skin friction and wall heat transfer rate.

5. CONCLUDING REMARKS

This paper presents a numerical study of time-dependent free convective flow of a Jeffrey viscoelastic fluid in the external boundary layer flow from a uniformly heated vertical cylinder. Graphical solutions are presented for the impact of two specific parameters i.e. Deborah

number β and Prandtl number Pr with fixed Jeffrey fluid parameter relaxation to retardation time ratio (λ). Based on the above results we have drawn the following conclusions:

1. The time required for attaining the steady-state is elevated with a rise in the values of Pr and β.
2. The velocity and temperature functions are reduced with increasing of Pr and decreasing values of β.
3. As β increases, the $\overline{C_f}$ magnitudes are enhanced and the reverse tendency is observed with increasing Pr. Similarly, $\overline{Nu}$ magnitudes are augmented with the rising values of Pr and the reverse trend is computed for β values.
4. Flow visualization shows that for increasing values of Deborah number, the streamlines and heat lines become closer to the hot wall whereas the isotherms increasingly move away from the wall.
5. The deviations of the heat lines from the hot wall decrease with higher values of Deborah number.
6. The transient and steady-state values of velocity, temperature, average wall shear stress (skin friction) and Nusselt number (wall heat transfer rate) for the Jeffrey fluid flow vary considerably from those computed for Newtonian fluids.

The current study has examined one type of rheological fluid, namely viscoelastic fluid. Future studies will consider alternate models including Eringen's micropolar model [44] and will be communicated imminently.

NOMENCLATURE

$\overline{C_f}$ average skin-friction coefficient

g acceleration due to gravity

$\overline{Nu}$ average Nusselt number

Gr Grashof number

Pr Prandtl number

k_1 thermal conductivity

r_0 radius of cylinder

r radial coordinate

R dimensionless radial coordinate

t' time

t dimensionless time

T' temperature

u, v velocity component in x, r direction

x axial coordinate

U, V dimensionless velocity component in X, R direction

X dimensionless axial coordinate

β_T volumetric coefficient of thermal expansion

Greek letters

θ dimensionless temperature

β Deborah number

Θ' heat function

μ dynamic viscosity

Ω dimensionless heat function

ψ dimensionless stream function

α thermal diffusivity of viscoelastic fluid

ρ density of viscoelastic fluid

υ kinematic viscosity of viscoelastic fluid

Subscripts

(i, j) grid level (X, R) coordinate system

w condition on the wall

k time step level

∞ free stream condition

ACKNOWLEDGEMENTS:

The first author wishes to thank DST-INSPIRE (Code No. IF160028) for the grant of research fellowship and to Central University of Karnataka for providing the research facilities. The authors wish to express their gratitude to the reviewers who highlighted important areas for improvement in this article. Their suggestions have served to enhance the clarity and depth of the interpretation in particular.

REFERENCES

1. A. Chandra and R.P. Chhabra "Flow over and forced convection heat transfer in Newtonian fluids from a semi-circular cylinder" *International Journal of Heat and Mass Transfer*, **54**, 225–241(2011).

2. P. Koteswara Rao, Akhilesh K. Sahu, and R. P. Chhabra, "Flow of Newtonian and power-law fluids past an elliptical cylinder: A Numerical Study", *Ind. Eng. Chem. Res.*, **49**, pp. 6649–6661 (2010).

3. Khan, W. A., Culham, J. R., and Yovanovich, M. M., "Fluid flow around and heat transfer from an infinite circular cylinder," *ASME J. Heat Transfer*, **127**, pp. 785–790(2005).

4. R.P. Bharti, R.P. Chhabra and V. Eswaran, "Steady flow of power-law fluids across a circular cylinder", *Can. J. Chem. Eng*. **84**, pp. 406–421(2006).

5. Lee, H. R., Chen, T. S., and Armaly, B. F., "Natural convection along slender vertical cylinders with variable surface temperature," *ASME J. Heat Transfer*, **110**, pp. 103–108 (1988).

6. P. Sivakumar, R.P. Bharti and R.P. Chhabra, "Steady flow of power-law fluids across an unconfined elliptical cylinder", *Chem. Eng. Sci*. **62**, pp.1682–1702(2007)

7. Chhabra, R. P., A. A. Soares and J. M. Ferreira "Steady non-Newtonian flow past a circular cylinder: a numerical study," *Acta Mech*. **172**, 1–16 (2004).

8. Shah, M. J., Petersen, E. E., and Acrivos, A. "Heat transfer from a cylinder to a power-law non-Newtonian fluid," *AIChemE J.*, **8**, pp. 542–549(1962).

9. G. J. Reddy, B. Kethireddy, M. Kumar and M. M. Hoque "A molecular dynamics study on transient non-Newtonian MHD Casson fluid flow dispersion over a radiative vertical cylinder with entropy heat generation" *Journal of Molecular Liquids*, **252**, 245-262 (2018).

10. G.J. Reddy, H. Ashwini and M. Kumar "Computational modelling of unsteady third-grade fluid flow over a vertical cylinder" *Results in Physics*, **8**, 671- 682 (2018).

11. O. Turan, A. Sachdeva, N. Chakraborty and R.J. Poole, Laminar natural convection of power-law fluids in a square enclosure with differentially heated side walls subjected to constant temperatures, *J. Non-Newtonian Fluid Mech*. **16**, pp. 1049–1063(2011).

12. G. Bin Kim, J. Min Hyun and H. Sang Kwak, Transient buoyant convection of a power-law non-Newtonian fluid in an enclosure, *Int. J. Heat Mass Transfer*, **46,** pp. 3605–3617(2003).

13. M. A. Sheremet and Ioan Pop, "Natural convection combined with thermal radiation in a square cavity filled with a viscoelastic fluid", *International Journal of Numerical Methods for Heat & Fluid Flow*, **28, pp.** 624–640 (2018).

14. G.J. Reddy, M. Kumar, J.C. Umavathi and M.A. Sheremet, "Transient entropy analysis for the flow of a second-grade fluid over a vertical cylinder", *Canadian Journal of Physics*, https://doi.org/10.1139/cjp-2017-0672

15. G.J. Reddy, M. Kumar, B. Kethireddy and A. J. Chamkha "Colloidal study of unsteady magnetohydrodynamic couple stress fluid flow over an isothermal vertical flat plate with entropy heat generation", *Journal of Molecular Liquids* 252, 169-179 (2018).

16. T. Hayat, S. Asad, M. Qasim and A. A. Hendi , "Boundary layer flow of a Jeffrey fluid with convective boundary conditions", *Int. J. Numer. Meth. Fluids*, **69**, pp. 1350-1362 (2012).

17. N. Santhosh and G. Radhakrishnamacharya, "Flow of Jeffrey fluid through narrow tubes" *International Journal of Scientific and Engineering Research*, **4**, ISSN 2229-5518 (2013).

18. B.K. Rao, "Heat transfer to non-Newtonian flows over a cylinder in cross flow", *International Journal Heat and Fluid Flow*, **21**, pp. 693-700 (2000).

19. P.V. S. Narayana and D. H. Babu, "Numerical study of MHD heat and mass transfer of a Jeffrey fluid over a stretching sheet with chemical reaction and thermal radiation", *Journal of the Taiwan Institute of Chemical Engineers*, **59**, pp. 1–8(2016)

20. M. Turkyilmazoglu and I. Pop, "Exact analytical solutions for the flow and heat transfer near the stagnation point on a stretching/shrinking sheet in a Jeffrey fluid", *International Journal of Heat and Mass Transfer*, **57**, pp. 82–88 (2013)

21. M. Y. Malik, I, Zehra and S. Nadeem, “Numerical treatment of Jeffrey fluid with pressure-dependent viscosity”, *Int. J. Num. Meth. Fluids*, **68**, 196–209 (2012).

22. T. Hayat, Q. Sajid, M. Farooq, A. Alsaed and M. Ayub, “Mixed convection flow of Jeffrey fluid along an inclined stretching cylinder with double stratification effect”, *Thermal Science*, **21**, pp. 849-862 (2017).

23. M. Y. Malik, A. Hussain, and S. Nadeem, “Flow of a Jeffery-six constant fluid between coaxial cylinders with heat transfer analysis”, *Communications in Theoretical Physics*, **56**, 345-351 (2011).

24. V. Ramachandra Prasad, S. Abdul Gaffar, E. Keshava Reddy, and O. Anwar Bég, “Flow and heat transfer of Jefferys non-Newtonian fluid from a horizontal circular cylinder”, *AIAA J. Thermophysics and Heat Transfer*, **28**, 764-770 (2014).

25. S. Sreenadh, M. M. Rashidi, K. Kumara Swamy Naidu and A. Parandhama, “Free convection flow of a Jeffrey fluid through a vertical deformable porous stratum”, *Journal of Applied Fluid Mechanics*, **9**, pp. 2391-2401 (2016).

26. S. Kimura and A, Bejan, “The heat line visualization of convective heat transfer”. *ASME Journal of Heat Transfer*, **105**, pp.916-919 (1983).

27. Bejan, A.: *Convection Heat Transfer*. 1st ed. New York: John Wiley and Sons (1984).

28. N.S. Bondareva, M.A. Sheremet, H.F. Oztop and N. Abu-Hamdeh, “Heatline visualization of natural convection in a thick walled open cavity filled with a nanofluid”, *International Journal of Heat and Mass Transfer*, **109**, pp. 175–186 (2017).

29. N.S. Bondareva, M.A. Sheremet, H.F. Oztop and N. Abu-Hamdeh, “Heatline visualization of MHD natural convection in an inclined wavy open porous cavity filled with a nanofluid with a local heater”, *International Journal of Heat and Mass Transfer*, **99**, pp. 872–881 (2016).

30. B. Pratibha, R. Monisha, S. Roy, and T. Basak, “Analysis of heatline based visualization for thermal management during mixed convection of hot/cold fluids within entrapped triangular cavities*” Journal of the Taiwan Institute of Chemical Engineers*, **77**, pp. 1-20 (2017).

31. R. Monisha, B. Pratibha, S. Roy, and T. Basak, “Heat flow visualization during mixed convection within entrapped porous triangular cavities with moving horizontal walls

via heat line analysis", *International Journal of Heat and Mass Transfer*, **108**, pp. 468-489 (2017).

32. Vinay Kumar., S.V.S.S.N.V.G. Krishna M. and B.V. Rathish K.: "Influence of MHD forces on Bejan's heat lines and mass lines in a doubly stratified fluid saturated Darcy porous enclosure in the presence of Soret and Dufour effects - A numerical study". *International Journal of Heat and Mass Transfer*, **117**, pp. 1041-1062 (2018).

33. G. J. Reddy, B. Kethireddy, J.C. Umavathi and M. A. Sheremet.: "Heat flow visualization for unsteady Casson fluid past a vertical slender hollow cylinder". *Thermal Science and Engineering Progress,* **5,** pp. 172–181(2018).

34. A. Morega, "The heat function approach to the thermomagnetic convection of electroconductive melts", *Revue roumaine des Sciences Techniques, Electrotechnique et Energetique,* **33**, pp. 359-368 (1988).

35. A. Alsaedi, Z. Iqbal, M. Mustafa, and T. Hayat "Exact solutions for the magnetohydrodynamic flow of a Jeffrey fluid with convective boundary conditions and chemical reaction", *Z. Naturforsch*. **67a**, 517 - 524 (2012).

36. T. Hayat, S. Asad, A. Alsaedi and F.E. Alsaadi "Radiative flow of Jeffrey fluid through a convectively heated stretching cylinder*", Journal of Mechanics,* **31**, pp. 69-78 (2015).

37. H.P. Rani, G. J. Reddy and C.N. Kim "Transient analysis of diffusive chemical reactive species for couple stress fluid flow over vertical cylinder*", Appl. Math. Mech. -Engl. Ed.*, **34**, 985-1000 (2013).

38. H.P. Rani, G. J. Reddy and C.N. Kim "Numerical analysis of couple stress fluid past an infinite vertical cylinder", *Engineering Applications of Computational Fluid Mechanics,* **5**, pp.159-169 (2011).

39. D. Tripathi and O. Anwar Bég, "Mathematical modelling of heat transfer effects on swallowing dynamics of viscoelastic flood bolus through the human oesophagus", *Int. J. Thermal Sciences*, **70**, 41-53 (2013).

40. V.R. Prasad, S. Abdul Gaffar, E. Keshava Reddy and O. Anwar Bég, "Numerical study of non-Newtonian boundary layer flow of Jeffreys fluid past a vertical porous plate in

a non-Darcy porous medium", *Int. J. Comp. Meth. Engineering Science & Mechanics,* **15** (4) 372-389 (2014).

41. V.R. Prasad, S. A. Gaffar, E. K. Reddy and O. Anwar Bég, "Numerical study of non-Newtonian Jeffreys fluid from a permeable horizontal isothermal cylinder in non-Darcy porous medium", *J. Braz. Soc. Mech. Sci. Eng.*, **37**, 1765-1783 (2015).
42. D. Tripathi, A. Yadav and O. Anwar Bég, "Electro-kinetically driven peristaltic transport of viscoelastic physiological fluids through a finite length capillary: mathematical modelling", *Mathematical Biosciences*, **283**, 155-168 (2017).
43. H. Schlichting, *Boundary-Layer Theory*, 7th edition, Mac-Graw-Hill, New York, USA (1979).
44. O. Anwar Bég, J. Zueco and T.B. Chang, Numerical analysis of hydromagnetic gravity-driven thin film micropolar flow along an inclined plane, *Chemical Engineering Communications,* **198**, 3, 312- 331 (2010).

TABLES

Table 1: The time required for various flow-field variables to attain the temporal peak and the time-independent state; the peak velocity for various control parameters pertaining to (a) Jeffrey fluid; (b) Newtonian fluid ($\beta = 0.0, \lambda = 0.0$).

			Temporal maximum (*t*) of			
Pr	**β**	**λ**	***U* (1,1.19)**	**θ(1,1.15)**	**Steady-state time(*t*)**	**Maximum velocity (*U*) at *X* = 1.0**
(a) Jeffrey fluid						
0.68	0.3	0.1	12.14	10.41	31.49	0.2379
0.68	0.5	0.1	15.54	13.43	34.74	0.1831
0.68	0.6	0.1	16.96	14.79	36.16	0.1726
0.68	0.8	0.1	19.82	17.61	38.71	0.1663
7.2	0.3	0.1	27.06	24.33	48.85	0.0905
(b) Newtonian fluid						
0.68	0.0	0.0	4.65	4.47	31.59	0.5003
7.2	0.0	0.0	7.90	7.38	37.25	0.2320

Table 2: Comparison between (a) Jeffrey fluid and (b) Newtonian fluid flows for various values of control parameters with respect to the average values of $-\overline{C_f}$ and $\overline{Nu}$.

	Pr	β	λ	$-\overline{C_f}$	$\overline{Nu}$
(a) Jeffrey fluid					
	0.68	0.3	0.1	2.6760	0.6867
	0.68	0.5	0.1	3.1295	0.6405
	0.68	0.6	0.1	3.2475	0.6245
	0.68	0.8	0.1	3.3641	0.6000
	7.2	0.3	0.1	1.0485	1.0363
(b) Newtonian fluid					
	0.68	0.0	0.0	0.8920	0.8523
	7.2	0.0	0.0	0.5576	1.4464

Table 3: Analysis of the time-step sensitivity for selecting time-step size.

Time step size (Δt)	Average skin-friction coefficient ($-\overline{C_f}$) for Pr = 0.68, β = 0.5 and λ = 0.1 .	Average Nusselt number ($\overline{Nu}$) for Pr = 0.68, β = 0.5 and λ = 0.1.
0.5	1.188643	0.892280
0.1	1.293957	0.806429
0.08	1.658031	0.778909
0.05	2.928810	0.702803
0.02	3.109601	0.660701
0.01	3.129592	0.640584

FIGURES

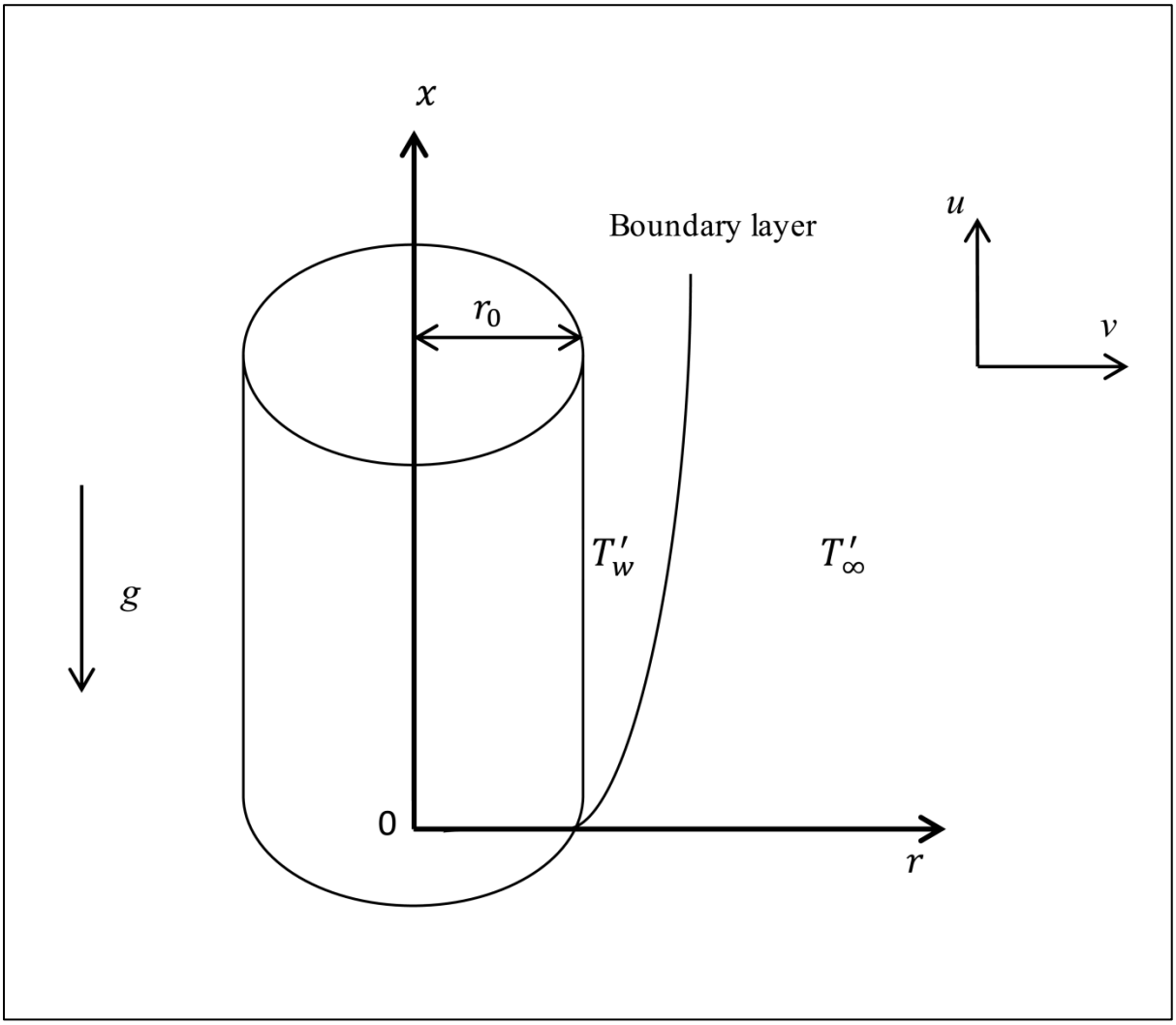

Figure 1: Schematic of the investigated problem and coordinate system.

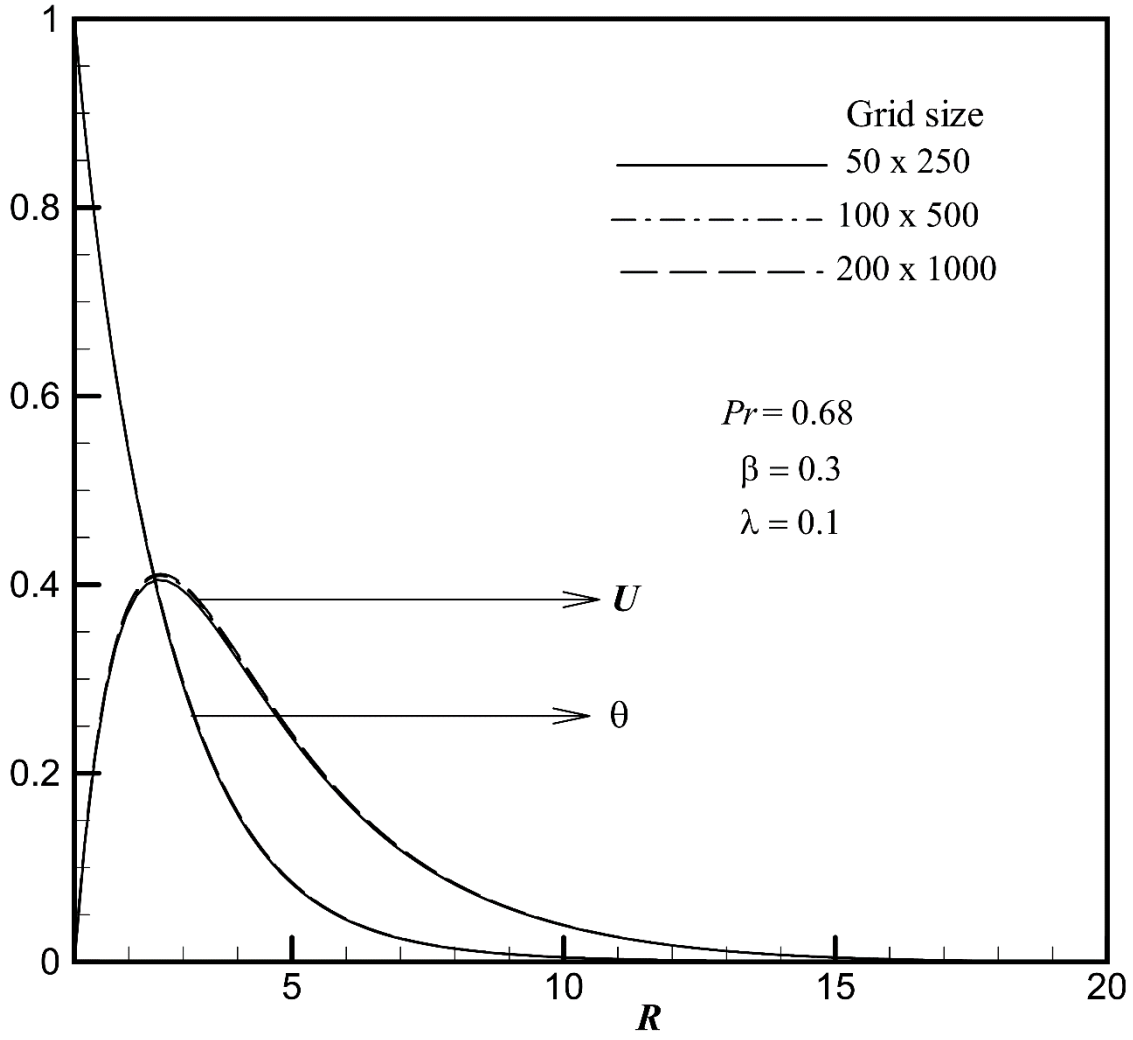

Figure 2: Grid independence test.

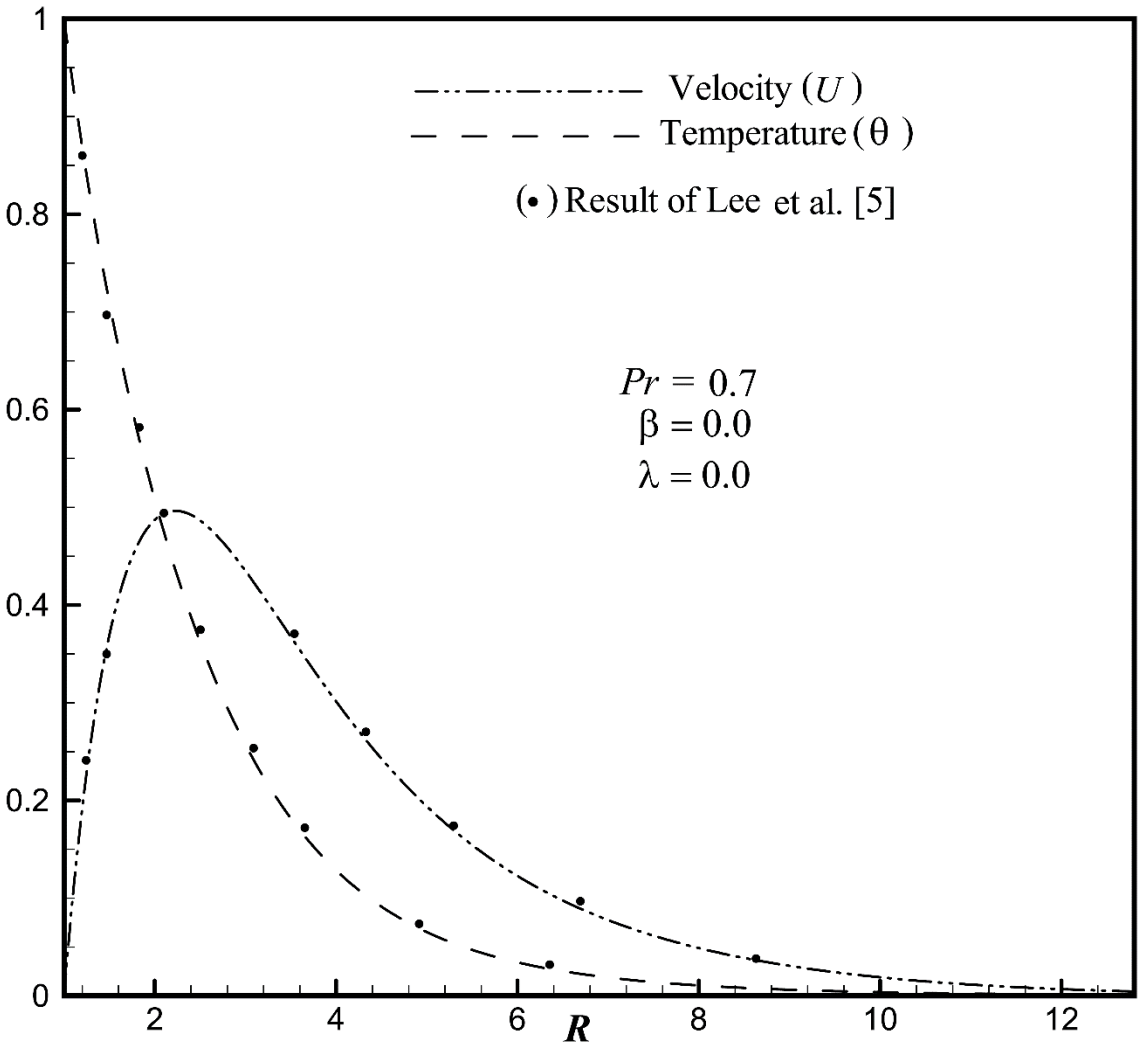

Figure 3: Comparison of the velocity and temperature profiles.

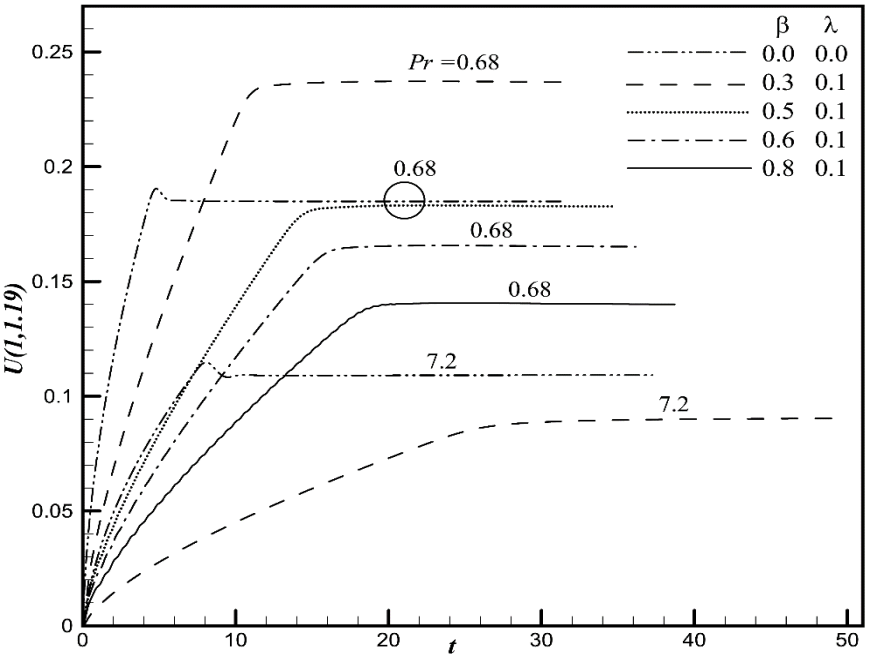
β λ
0.0 0.0
0.3 0.1
0.5 0.1
0.6 0.1
0.8 0.1
Pr =0.68
0.68
0.68
0.68
7.2
7.2
U(1,1.19)
t
0
0.05
0.1
0.15
0.2
0.25
0
10
20
30
40
50

4(a)

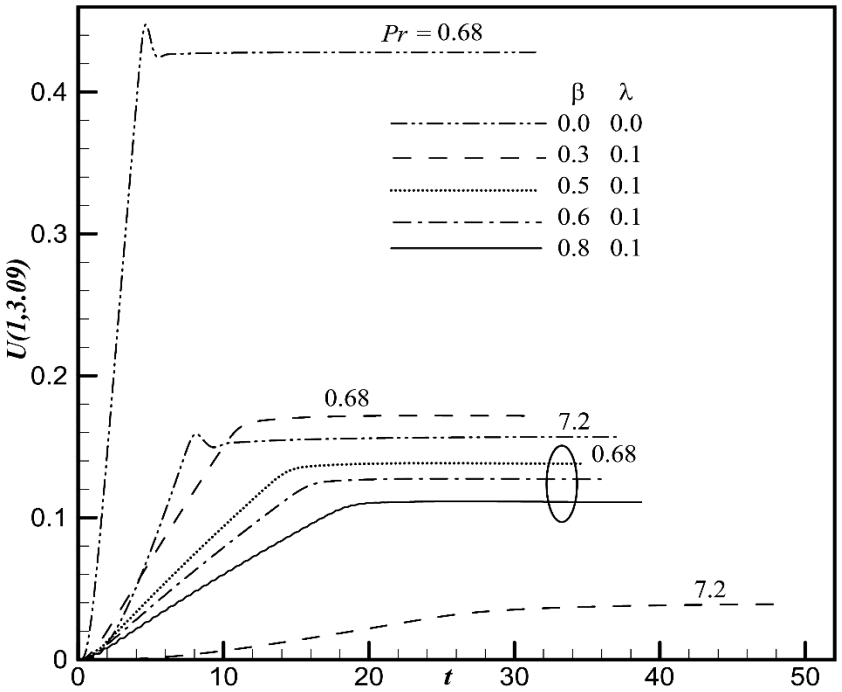
Pr = 0.68
β λ
0.0 0.0
0.3 0.1
0.5 0.1
0.6 0.1
0.8 0.1
0.68
7.2
0.68
7.2
U(1,3.09)
t
0
0.1
0.2
0.3
0.4
0
10
20
30
40
50

4(b)

Figure 4: The simulated transient velocity profile (*U*) against time *t* for different values of *Pr* and β at the point (a) (1, 1.19); (b) (1, 3.09).

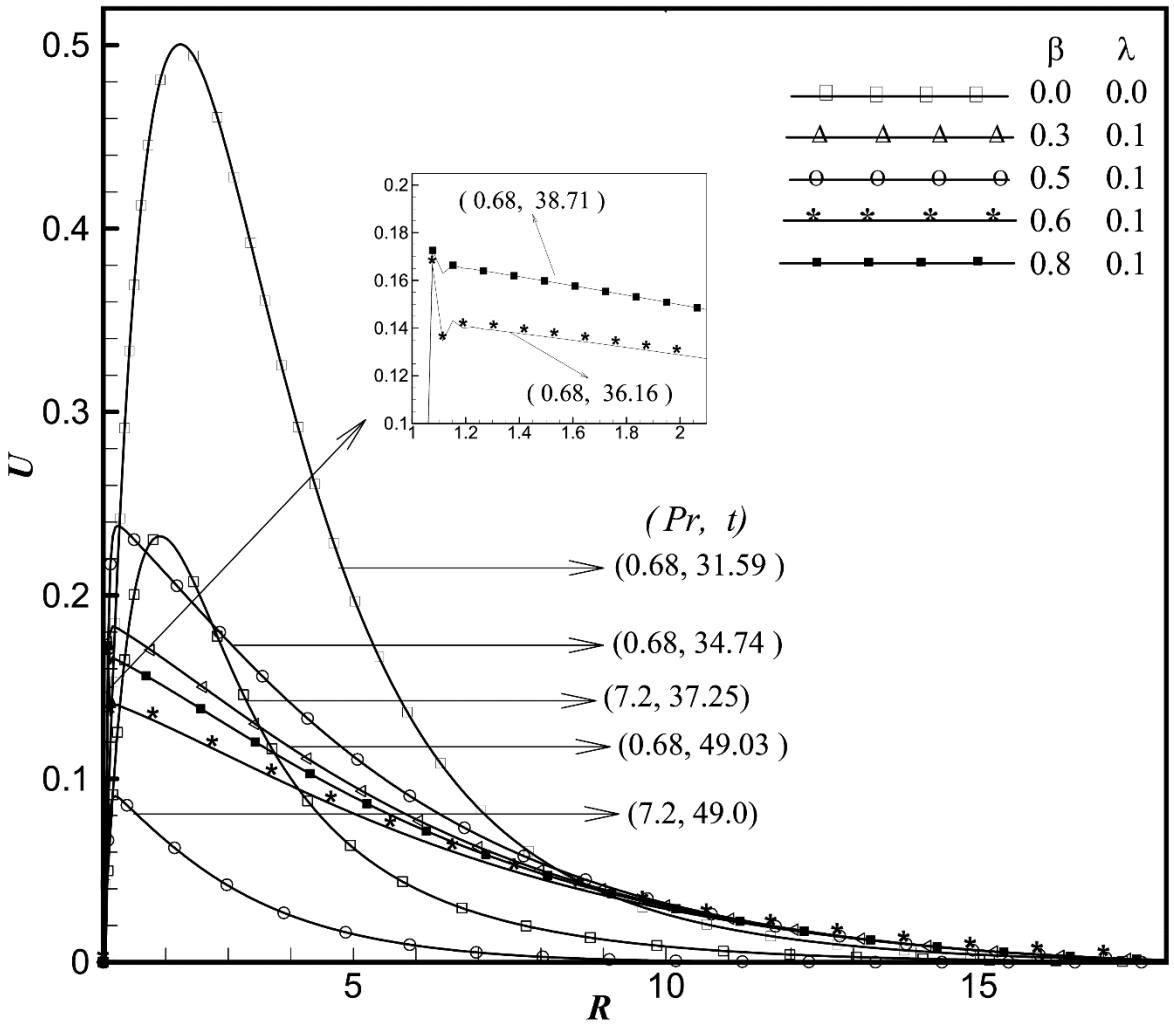

Figure 5: The simulated steady-state velocity profile (*U*) against *R* at *X* = 1.0 for different values *Pr* and β.

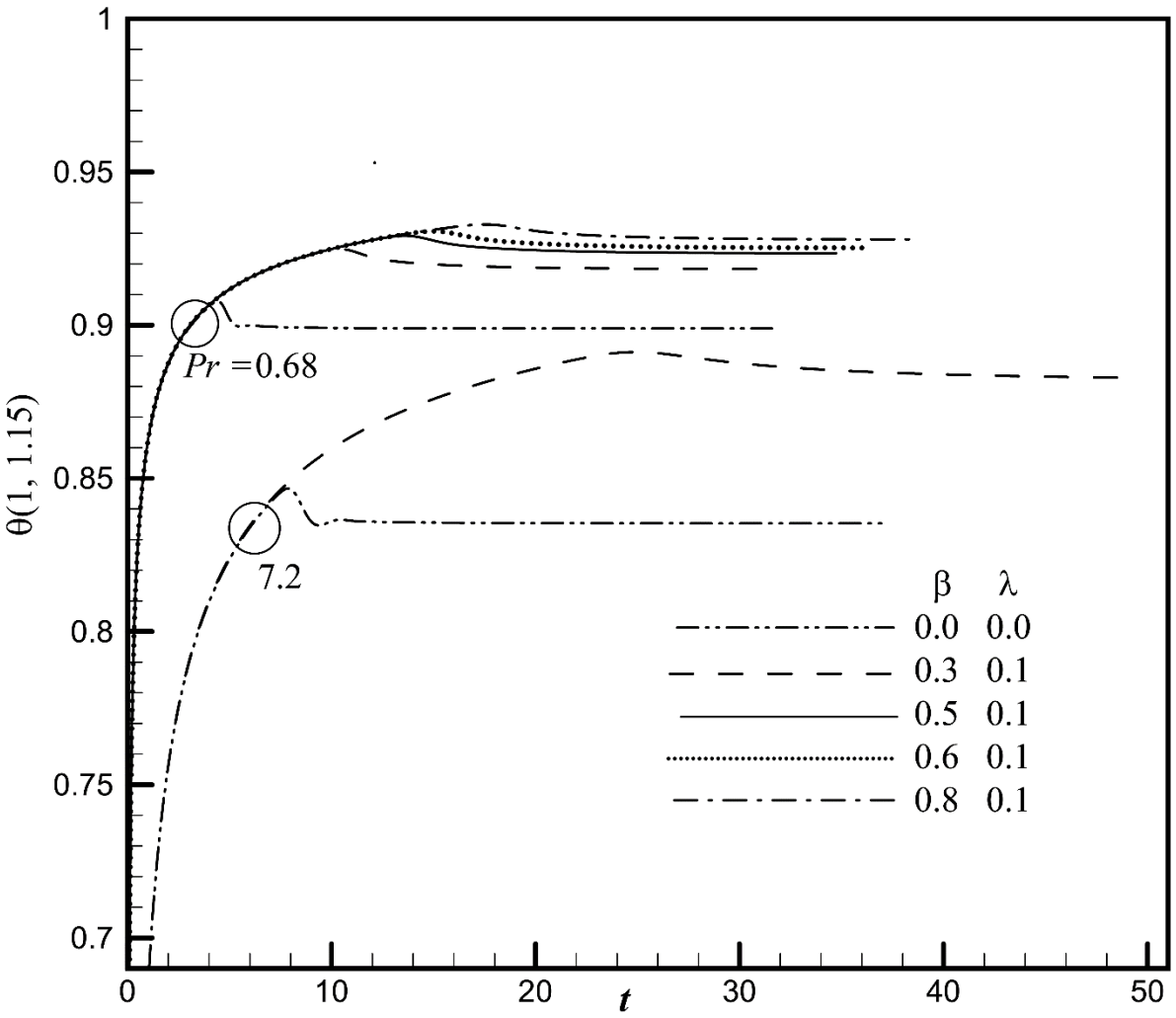

Figure 6: The simulated transient temperature (θ) against time *t* at the point (1, 1.15) for different values of *Pr* and β.

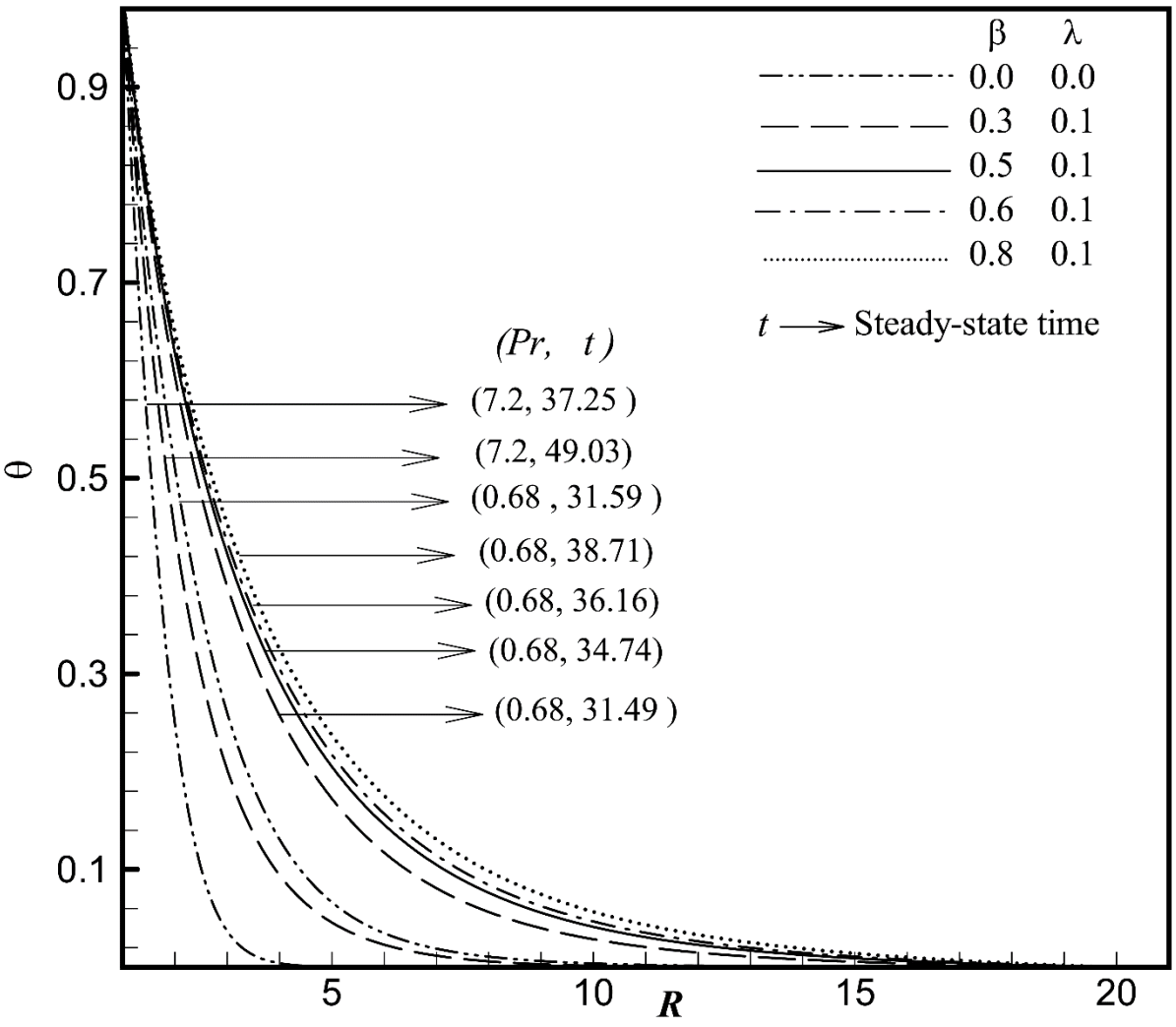

Figure 7: The simulated steady state temperature profile (θ) against R at X = 1.0 for different values of Pr and β.

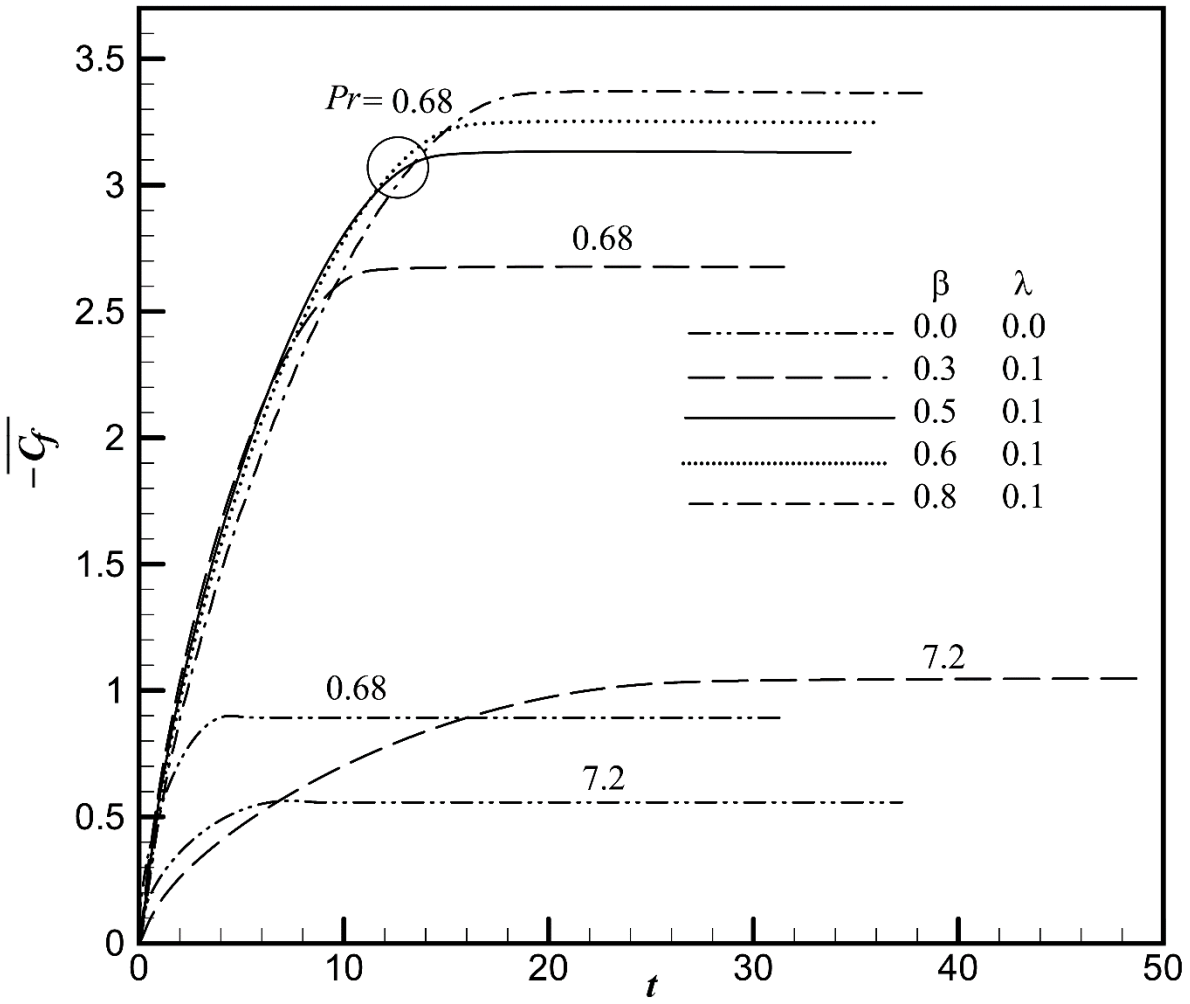

Figure 8: The simulated average skin friction ($\overline{C_f}$) for different values of *Pr* and β.

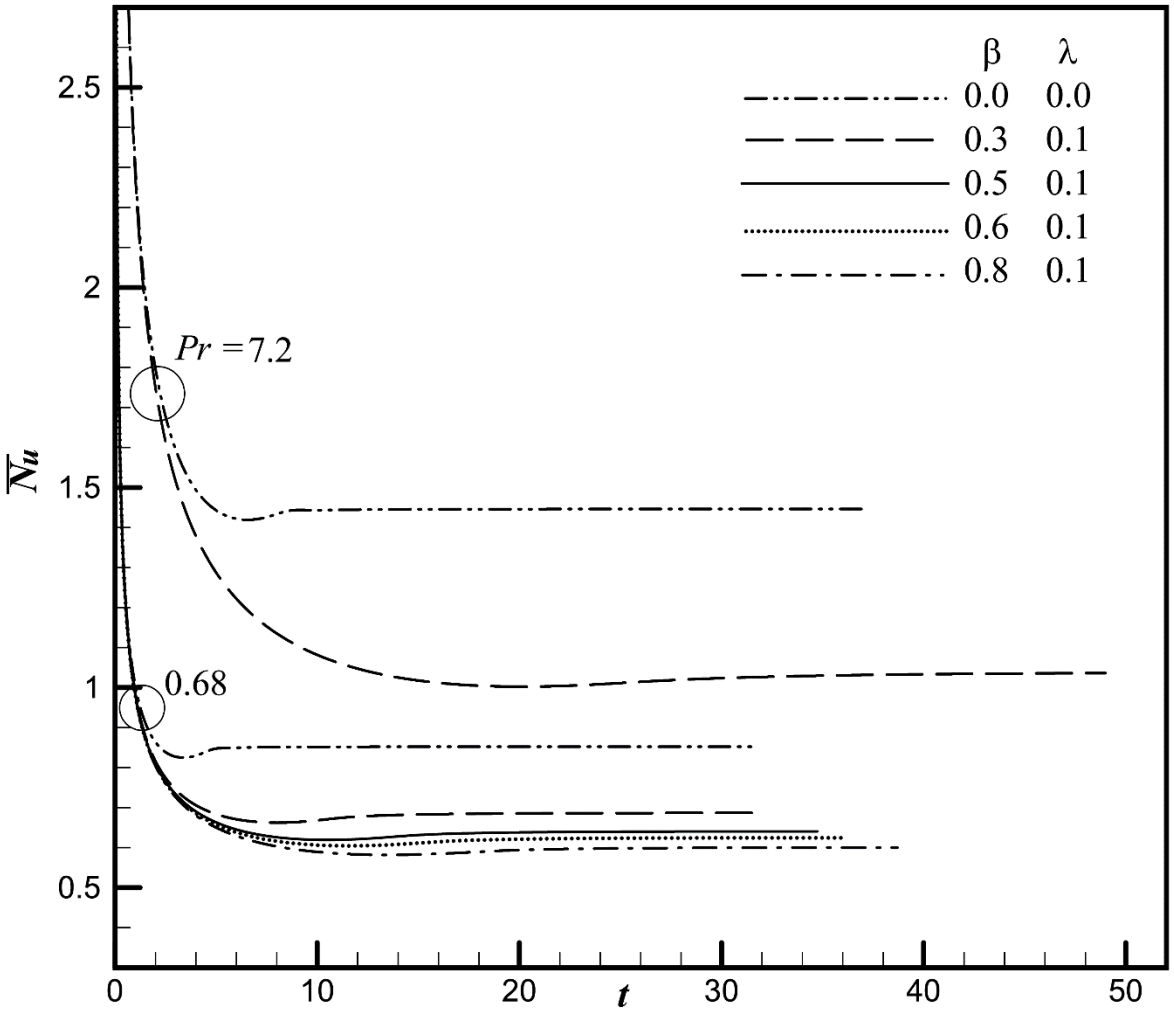

Figure 9: The simulated average Nusselt number ($\overline{Nu}$) for different values of *Pr* and β.

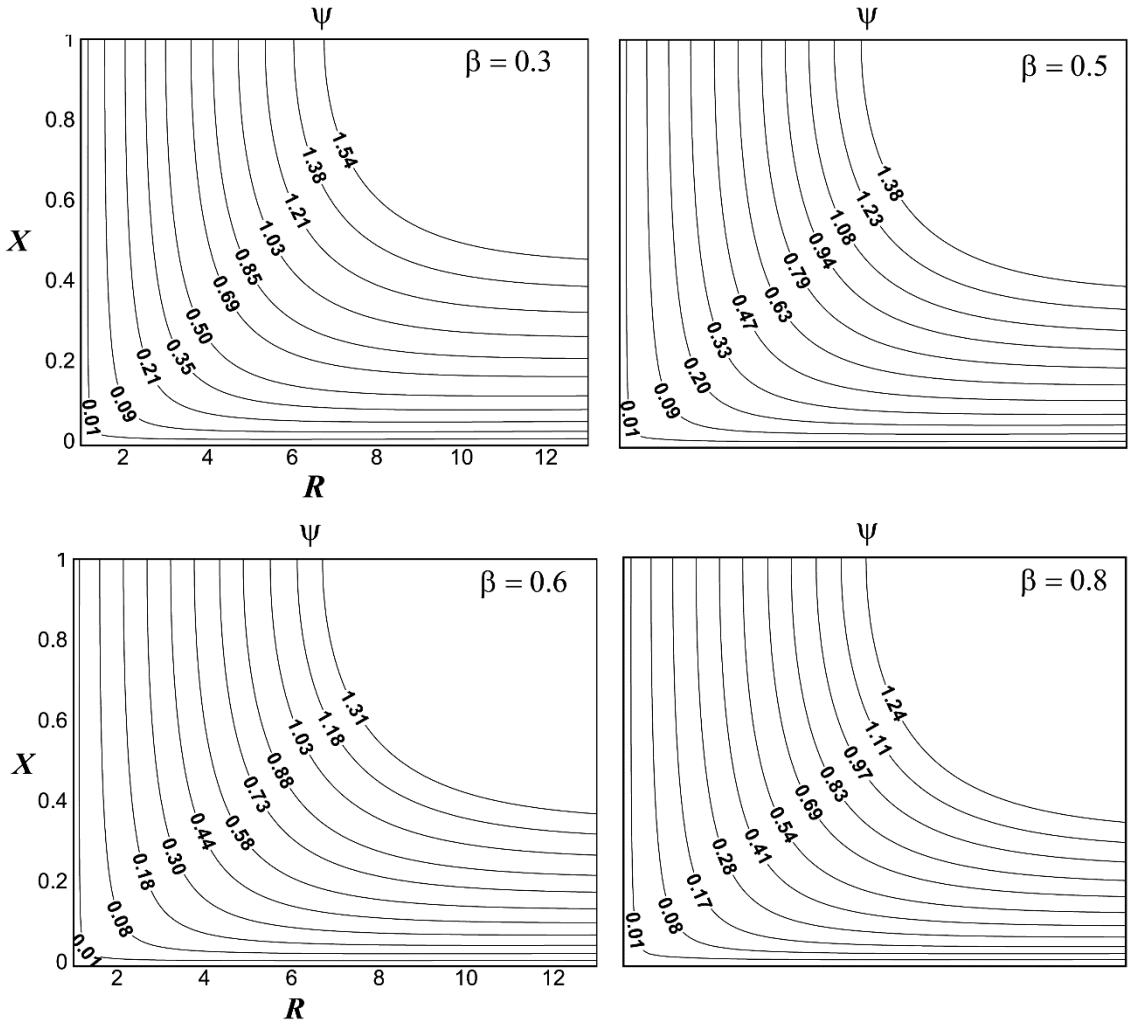
ψ
β = 0.3
1.54
1.38
1.21
1.03
0.85
0.69
0.50
0.35
0.21
0.09
0.01
X
R
ψ
β = 0.5
1.38
1.23
1.08
0.94
0.79
0.63
0.47
0.33
0.20
0.09
0.01
ψ
β = 0.6
1.31
1.18
1.03
0.88
0.73
0.58
0.44
0.30
0.18
0.08
0.01
X
R
ψ
β = 0.8
1.24
1.11
0.97
0.83
0.69
0.54
0.41
0.28
0.17
0.08
0.01

(10a)

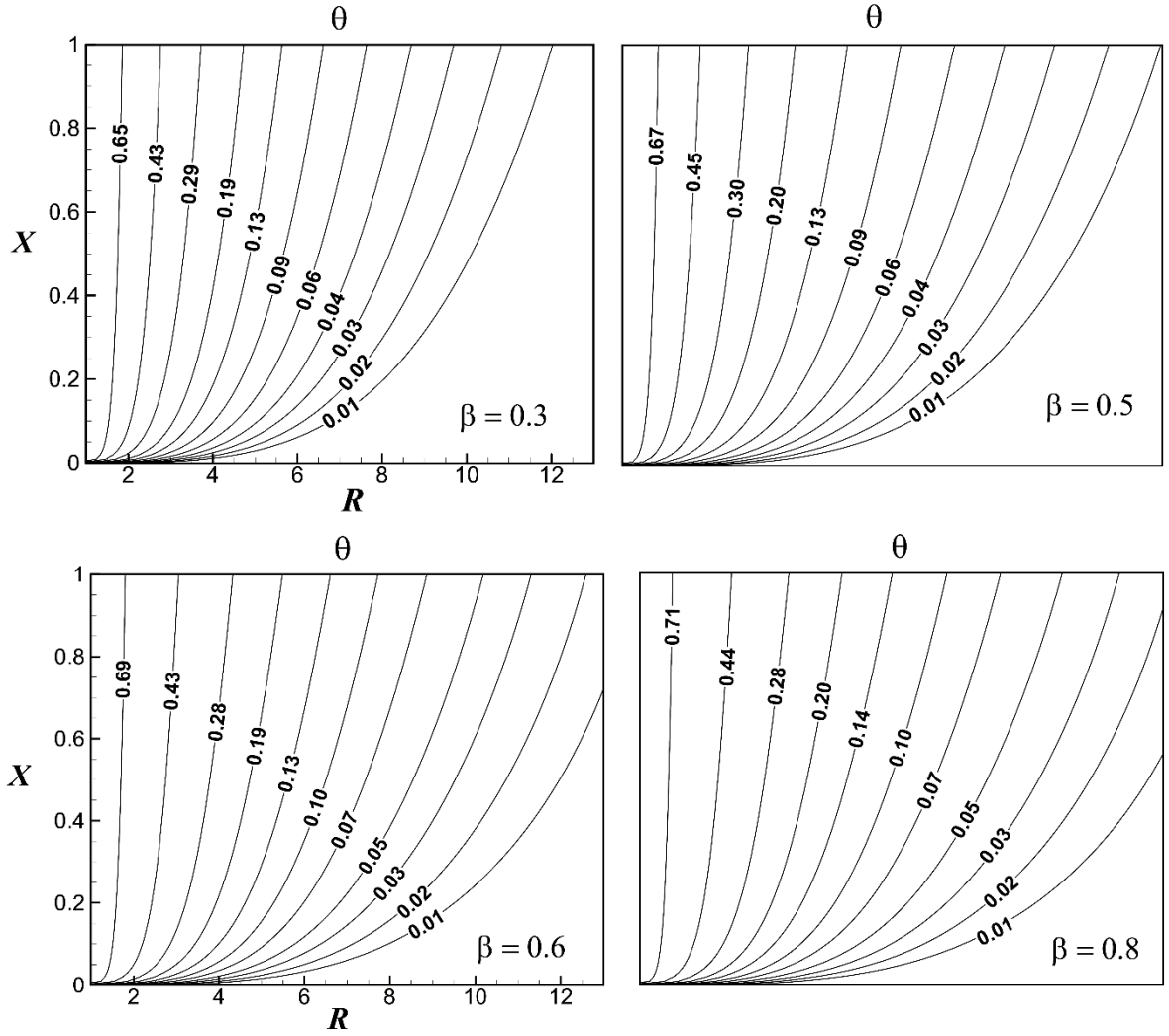
θ
θ
θ
θ
X
R
β = 0.3
β = 0.5
β = 0.6
β = 0.8
0.65
0.43
0.29
0.19
0.13
0.09
0.06
0.04
0.03
0.02
0.01
0.67
0.45
0.30
0.20
0.13
0.09
0.06
0.04
0.03
0.02
0.01
0.69
0.43
0.28
0.19
0.13
0.10
0.07
0.05
0.03
0.02
0.01
0.71
0.44
0.28
0.20
0.14
0.10
0.07
0.05
0.03
0.02
0.01

(10b)

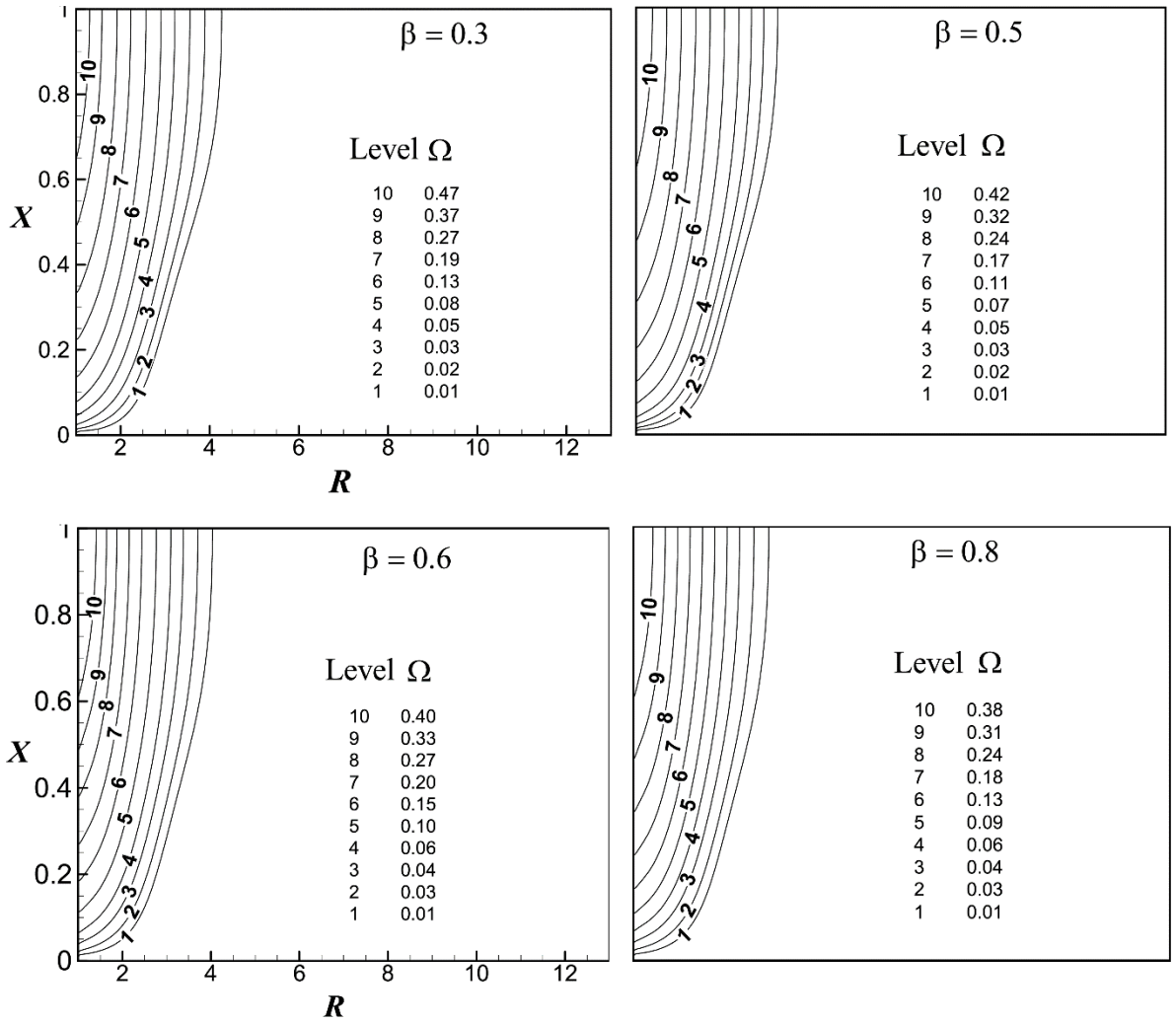

(10c)

Figure 10: Steady-state (a) streamlines (Ψ), (b) isotherms (θ) and (c) heat lines (Ω) for different values of β and fixed values of Pr = 0.68, $\lambda = 0.1$.

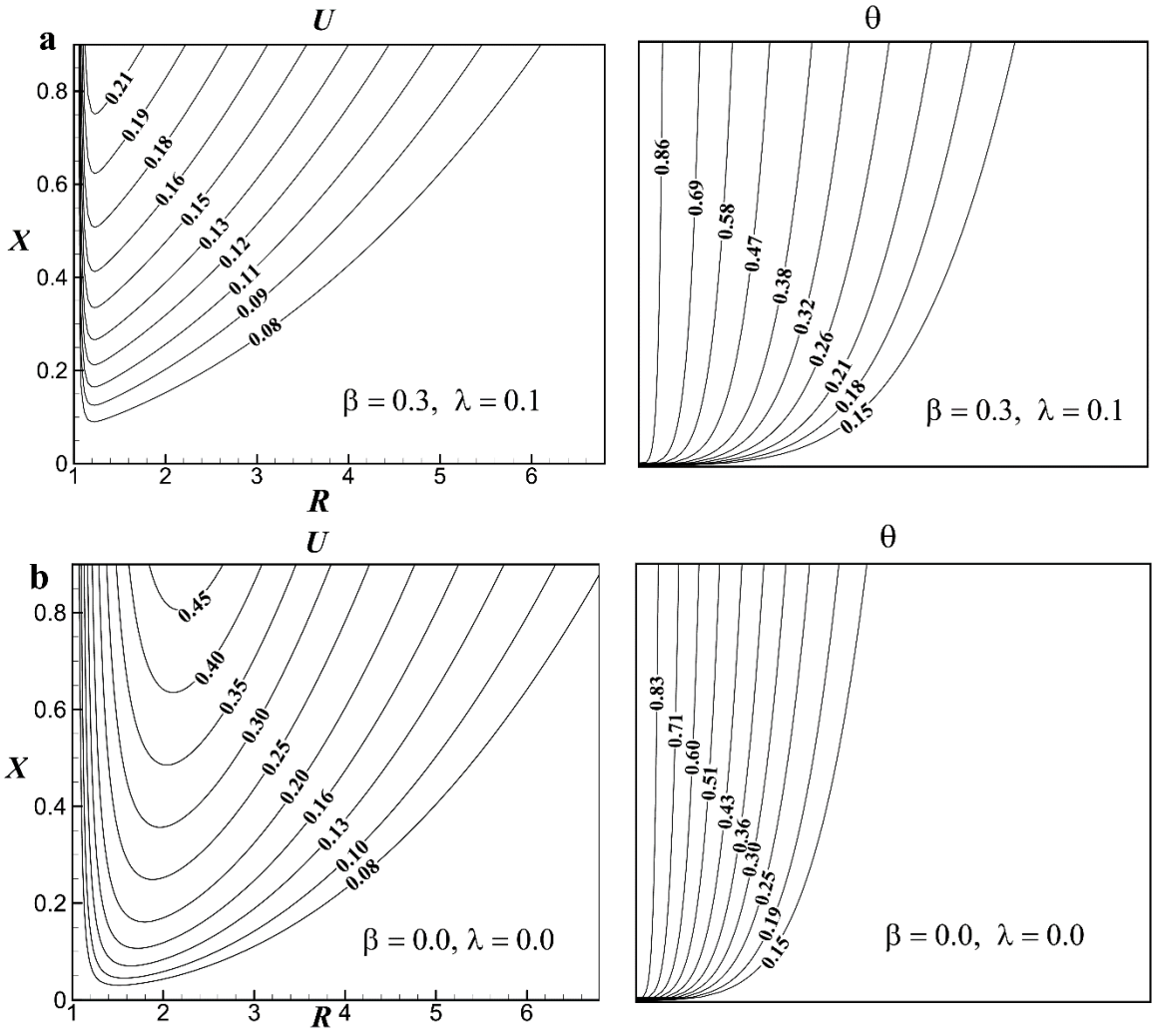

Figure 11: Steady-state velocity (U) and temperature (θ) contours with Pr = 0.68, (a) Jeffrey fluid (b) Newtonian fluid.